PHYSICAL REVIEW C VOLUME 24, NUMBER 3 SEPTEMBER 1981

Effective nucleon-nucleon interaction for scattering at intermediate energies

W. G. Love
Department of Physics and Astronomy, University of Georgia, Athens, Georgia 30602
and Los Alamos National Laboratory, Los Alamos, New Mexico 87545

M. A. Franey
Department of Physics, University of Minnesota, Minneapolis, Minnesota 55455
(Received 23 February 1981)

A local representation of the free nucleon-nucleon t matrix has been determined for several projectile bombarding energies between 100 and 800 MeV/nucleon and is presented in tabular form. The form of the interaction has been tailored for use in calculations of elastic and inelastic proton scattering in this energy range. The technique used to derive the interaction is outlined and some of the resulting uncertainties are discussed. A number of the most important properties of the interaction and their roles in the calculation of nucleon-nucleus scattering observables are discussed. A few applications of the interaction are made to a variety of (p,p') transitions within a single-scattering context.

[NUCLEAR REACTIONS An energy-dependent multiple Yukawa representation of the on-shell nucleon-nucleon t matrix between 100 and 800 MeV.]

I. INTRODUCTION

A critical ingredient for calculating and interpreting nucleon-nucleus scattering at intermediate energies is a knowledge of the coupling between the projectile and the target nucleons. Because of the nucleon's spin, isospin, and indistinguishability from the target nucleons, it is simultaneously a rich and complex probe. A quantitative knowledge of the nucleon-nucleon (N-N) coupling from first principles over a wide energy range must await a more complete theory of strong interactions. For the present we must be content with a more phenomenological approach, namely that of obtaining the N-N coupling from measurements of N-N scattering observables. Even if the bare coupling between two nucleons were known, it would likely be too strong for use in perturbation theory and would have to be transformed into an operator like a G matrix before being used as a practical tool for the interpretation of nucleon-nucleus scattering. This is basically the route taken at lower energies[1-3] where phenomenological N-N potentials are available.

It was suggested some time ago that some version of the impulse approximation (IA) might be appropriate for understanding nucleon-nucleus scattering at nucleon bombarding energies (E_P) above ~ 100 MeV. Indeed, one of the primary motivations for extending proton-scattering measurements to intermediate energies has been to circumvent many of the complicated reaction mechanisms known to obscure the interpretation of nucleon-nucleus scattering at lower bombarding energies. In the impulse approximation[4,5] the effective interaction between the incident nucleon and each of the target nucleons is taken to be the free N-N t matrix. The appeal of this approach is clear; we can regard the coupling as known and focus our attention on obtaining nuclear structure information.

Because of the strong coupling between the projectile and the target, the effects of optical model distortion are essential for quantitative comparisons of theoretical calculations with experimental data at intermediate energies, and we will refer to the distorted-wave impulse approximation (DWIA) when making such comparisons. A number of failures and successes of the DWIA at intermediate

energies have already been reported,[6–9] especially below $E_P \simeq 200$ MeV, where the effects due to Fermi averaging and Pauli blocking are most important. Nevertheless, it is widely believed that the IA should provide a reasonable starting point at intermediate energies; we must be prepared to make corrections where necessary, and hopefully these will teach us something.

Although the IA has been used for a number of years,[4,5] a rather complete set of phase shifts[10] between 200 and 500 MeV has only recently become available. Moreover, there is currently becoming available large amounts of experimental data on a variety of observables for nucleon-nucleus scattering over a large part of the energy range between 100 and 800 MeV. In light of these developments it seems appropriate to construct an effective interaction based on the free N-N t matrix which can be used as a starting point to help interpret these data. It is evident that as more complete N-N information becomes available, especially above 500 MeV, the present interaction will likely have to be updated.

II. THE EFFECTIVE INTERACTION

A. Method of derivation

The precise relationship between N-N data and a reasonable effective interaction (V) for nucleon-nucleus scattering is generally not a simple one. In the IA (as described here) we start from the free phenomenological N-N scattering amplitude (M) which, at each nucleon-bombarding energy, is obtained from a phase-shift analysis essentially as described in Ref. 11. In order to incorporate the well-established (peripheral) part of the N-N amplitude, the complete amplitude is written as

$$M = M(\delta, J_{\max}) + M^P - M^{PS}(J_{\max}) \ , \tag{1}$$

where $M(\delta, J_{\max})$ is that part of the amplitude arising from the phase-shift expressions for states having a total angular momentum of $0 \le J \le J_{\max}$. M^P is the total (all J) one-pion-exchange contribution (OPEC) in Born approximation and M^{PS} represents that part of M^P acting in states where $0 \le J \le J_{\max}$. $M(\delta, J_{\max})$ is determined phenomenologically by a phase-shift analysis[11,12] of the available N-N data, and between 100 and 800 MeV $J_{\max}$ is typically 6. Following Arndt,[12] the OPEC for $J = J_{\max} + 1$ through $J = J_{\max} + 3$ is unitarized. Table I shows the source of phases used in this work to construct the amplitudes at each energy.

TABLE I. Phase-shift sources.

Energy (MeV)	Source	Set
100	a	CK80, 6/80
140	a	CK80, 6/80
210	b	
325	b	$\chi^2 = 432.5$
425	b	
515	b	
650	a	C650, 9/80
800	a	CL80, 6/80

[a]Reference 12.
[b]Reference 10.

1. *The structure of the N-N amplitudes*

The N-N amplitudes can be expressed[4] as

$$M(E_{\text{c.m.}}, \theta) = A + B\,\vec{\sigma}_1\cdot\hat{n}\,\vec{\sigma}_2\cdot\hat{n} + C(\vec{\sigma}_1 + \vec{\sigma}_2)\cdot\hat{n} + E\,\vec{\sigma}_1\cdot\hat{q}\,\vec{\sigma}_2\cdot\hat{q} + F\,\vec{\sigma}_1\cdot\hat{Q}\,\vec{\sigma}_2\cdot\hat{Q} \ , \tag{2}$$

where A, B, C, E, and F are functions of: $E_{\text{c.m.}}$, the center-of-mass energy; θ, the scattering angle in the c.m. system; and T, the total two-body isospin. If $\vec{k}$ ($\vec{k}'$) is the initial (final) momentum of either particle in the c.m. system, then the unit vectors $[\hat{q}, \hat{Q}, \hat{n}]$ form a right-handed coordinate system with

$$\vec{q} = \vec{k} - \vec{k}', \ \vec{Q} = \vec{k} + \vec{k}' \ , \qquad q = 2k\sin(\theta/2), \ Q = 2k\cos(\theta/2) \ . \tag{3}$$

To identify the spin and spatial ranks of the various parts of the N-N amplitude we use the identity

$$\vec{\sigma}_1\cdot\hat{u}\,\vec{\sigma}_2\cdot\hat{u} = \tfrac{1}{3}[S_{12}(\hat{u}) + \vec{\sigma}_1\cdot\vec{\sigma}_2] \ , \tag{4}$$

and the completeness of $[\hat{q}, \hat{Q}, \hat{n}]$, giving

$$M(E_{\text{c.m.}}, \theta) = A'P_S + B'P_T + C(\vec{\sigma}_1 + \vec{\sigma}_2)\cdot\hat{n} + E'S_{12}(\hat{q}) + F'S_{12}(\hat{Q}) \ , \tag{5}$$

where S_{12} is the usual tensor operator, P_S (P_T) is the singlet (triplet) spin-projection operator, and

$$A' = A - B - E - F, \ B' = A + \frac{B + E + F}{3} \ , \qquad E' = \frac{E - B}{3} \ , \ F' = \frac{F - B}{3} \ . \tag{6}$$

The amplitudes A' and B' are the central parts of M; the C term, which is linear in the Pauli spin matrices, is a spin-orbit-like term, and E' and F' are the tensor parts of M.

Rather than work with the amplitude, we choose to work with the N-N t matrix, which is more directly related to effective interactions derived using other techniques[6] such as the construction of G matrices, etc. This relationship is

$$t_{NN}(E_{\text{c.m.}},\theta) = \eta M(E_{\text{c.m.}},\theta) \ , \tag{7}$$

$$\eta = \frac{-4\pi(\hbar c)^2}{E_{\text{c.m.}}} \ , \quad E_{\text{c.m.}}{}^2 = m^2c^4 + (\hbar ck)^2 \ .$$

We note that the t matrix defined here is larger than that defined in Ref. 6 by a factor of $(2\pi)^3$.

2. *Different approaches to the use of t as an effective interaction*

For the calculation and interpretation of nucleon-nucleus scattering it is desirable to have an effective interaction that is simple and yet realistic enough to represent the important and interesting characteristics of the free N-N t matrix. Since these objectives are not strictly compatible, some compromise is necessary, and this has led to different approaches for using the free t matrix as an effective "interaction" in the IA.

The simplest approach[5] is that of taking the effective interaction V to be

$$V_{12} = t_{NN}(E,q)\delta(\vec{r}_{12}) \ , \tag{8}$$

where E and q and each of the unit vectors in Eq. (2) are assigned their asymptotic values. This approximation should be best at small q and large E, where refractive effects are small. For momentum transfers $q > 2k \sim k_A$ (which corresponds to a scattering angle of $\sim 60°$ in the nucleon-nucleus system), t must be extrapolated off shell; k_A is the incident nucleon's momentum in the nucleon-nucleus c.m. system [see Eqs. (19)]. In this approach, the extrapolation at large q is typically made by representing t_{NN} by a Gaussian or other simple form at small q. Implicit in the use of this approximation is the assumption that antisymmetrization between the projectile and target nucleus is adequately represented by using the antisymmetrized free N-N t matrix. That this need not necessarily be the case is illustrated by a simple example. Consider (nonrelativistically for simplicity) the scattering of two nucleons by a singlet-even interaction $V(r)$. To first order in V, the t matrix in the N-N system is

$$t_{NN} = \tilde{V}(q) + \tilde{V}(Q), \ \ Q^2 = 4k^2 - q^2 \ , \tag{9}$$

where $\tilde{V}(q)$ is the Fourier transform of $V(r)$ representing the direct term and $\tilde{V}(Q)$ represents the exchange term. The corresponding t matrix in the nucleon-nucleus (N-A) system can to a good approximation[1] be written as

$$t_{NA} = \tilde{V}(q) + \tilde{V}(k_A) \ . \tag{10}$$

That is, to a good approximation the momentum transfer required for the exchange term in the N-A system is just that associated with stopping the incident nucleon. Although these two expressions will give similar results when used in Eq. (8) for small q where $Q \sim 2k \sim k_A$, they can give quite different results for q appreciably different from zero. The two expressions above are only strictly equivalent when V is a δ function and $\tilde{V}(q)$ is constant.

An approximation[13] quite similar to that embodied in Eq. (8) is obtained by assuming a local finite-range form for the effective interaction $V_{12} \rightarrow V(\vec{r}_{12})$ and then requiring $\tilde{V}(q)$ to equal t_{NN} as closely as possible. It should be noted that a local ansatz for V_{12} precludes terms of the type F' in Eq. (5) and in this sense is incomplete. This procedure can, however, yield all of the other *types* of terms in Eqs. (2) and (5) provided V_{12} includes two-body spin-orbit and static tensor terms.

For simplicity and computational feasibility it is highly desirable to represent $t_{NN}(E,q)$ by a local coordinate space interaction in the N-N system. It is possible to do this and to include all of the different types of terms in Eq. (5) provided we include antisymmetrization explicitly in both the N-N and N-A systems and this is the approach[6] adopted here. To the extent that most of the energy dependence of t_{NN} arises from antisymmetrization, this technique should permit the use of a single t_{NN} over a wider range of energies than the techniques mentioned above. In this work we try to represent V_{12} in each N-N channel (triplet-odd, triplet-even, etc.) by

$$V_{12} = V^C(r_{12}) + V^{LS}(r_{12})\vec{L}\cdot\vec{S} + V^T(r_{12})S_{12} \ , \tag{11}$$

where $\vec{L}\cdot\vec{S}$ and S_{12} are the usual spin-orbit and tensor operators. More specifically, the parameters of V_{12} are adjusted until

$$t_{NN}(E,q) = \int d^3r\, e^{-i\vec{k}'\cdot\vec{r}} V_{12}[1 + (-)^l P^x] e^{i\vec{k}\cdot\vec{r}} \tag{12}$$

within satisfactory limits. Here P^x is the space exchange operator which changes $\vec{r} \rightarrow -\vec{r}$ on the right and $(-)^l$ (with l = relative angular momentum in the N-N system) ensures antisymmetrization. For computational simplicity and to reflect the exchange of various mesons, the radial parts of the central and spin-orbit components of V are taken to be a sum of Yukawa forms; the radial shape of the tensor term is taken to be r^2 times a sum of Yukawa terms. In particular,

$$V^C(r) = \sum_{i=1}^{N_C} V_i^C Y(r/R_i), \quad Y(x) = e^{-x}/x \tag{13a}$$

$$V^{LS}(r) = \sum_{i=1}^{N_{LS}} V_i^{LS} Y(r/R_i) \ , \tag{13b}$$

$$V^T(r) = \sum_{i=1}^{N_T} V_i^T r^2 Y(r/R_i) \ , \tag{13c}$$

where the V's are complex strengths. For the real central part of the interaction the Yukawa term of longest range is fixed to be that of the long-range part of the one-pion-exchange potential (OPEP). The longest-range term in the tensor interaction was fixed at 0.7 fm since this form has roughly the same distribution of small ($q \lesssim 1$ fm^{-1}) Fourier components as does the tensor part of the OPEP. The strength of the 0.7-fm term was not constrained to match the OPEP; this was found to be too restrictive. A range parameter of 0.4 fm was included at all energies, in part to crudely simulate multiple-pion exchange processes present in theoretically based *potentials*. The other range parameters were chosen primarily for convenience and flexibility. Inserting Eqs. (13) into Eq. (12) we find

$$t_{NN}(E,q) = [\tilde{V}_S^C(q) + (-)^l \tilde{V}_S^C(Q)]P_S + [\tilde{V}_T^C(q) + (-)^l \tilde{V}_T^C(Q)]P_T + \frac{i}{4}[Q\tilde{V}^{LS}(q) - (-)^l q\tilde{V}^{LS}(Q)](\vec{\sigma}_1 + \vec{\sigma}_2)\cdot\hat{n} - [\tilde{V}^T(q)S_{12}(\hat{q}) + (-)^l \tilde{V}^T(Q)S_{12}(\hat{Q})] \ . \tag{14}$$

The Fourier transforms ($\tilde{V}$) are defined by

$$\tilde{V}^C(k) = 4\pi \int_0^\infty r^2 dr\, j_0(kr) V^C(r) = 4\pi \sum_i \frac{V_i^C R_i^3}{1 + (kR_i)^2} \ , \tag{15a}$$

$$\tilde{V}^{LS}(k) = 4\pi \int_0^\infty r^3 dr\, j_1(kr) V^{LS}(r) = 8\pi \sum_i \frac{V_i^{LS} k R_i^5}{[1 + (kR_i)^2]^2} \ , \tag{15b}$$

$$\tilde{V}^T(k) = 4\pi \int_0^\infty r^2 dr\, j_2(kr) V^T(r) = 32\pi \sum_i \frac{V_i^T k^2 R_i^7}{[1 + (kR_i)^2]^3} \ , \tag{15c}$$

where $k = q$ or Q. Combining Eqs. (5), (7), and (14) we find

$$t_S^C \equiv \tilde{V}_S^C(q) + (-)^l \tilde{V}_S^C(Q) = \eta A' \ , \tag{16a}$$

$$t_T^C \equiv \tilde{V}_T^C(q) + (-)^l \tilde{V}_T^C(Q) = \eta B' \ , \tag{16b}$$

$$4t^{LS} \equiv Q\tilde{V}^{LS}(q) - (-)^l q\tilde{V}^{LS}(Q) = -4i\eta C \ , \tag{16c}$$

$$t^T \equiv \tilde{V}^T(q) = -\eta E', \quad \tilde{V}^T(Q) = (-)^{l+1}\eta F' \ . \tag{16d}$$

On the energy shell, q and Q are not independent and Eq. (16d) implies

$$E'(\pi - \theta) = (-)^l F'(\theta) = (-)^T F'(\theta) \ , \tag{17}$$

where T is the total N-N isospin. This is the appropriate interdependence of these amplitudes for the scattering of nucleons in an isospin representation.

Apart from the OPEP constraints mentioned earlier, the interaction strengths (V_i) were determined via a χ^2 search procedure using Eqs. (15) and (16). For simplicity, the search was performed as a function of the angle (in the N-N system) at 5° steps between 0° and 180°. With the exception of the tensor amplitudes in Eq. (11), which are neither symmetric nor antisymmetric about 90°, χ^2 was computed via

$$\chi^2 = \sum_i [M_p(E,\theta_i) - M_c(E,\theta_i)]^2 \ , \tag{18}$$

where M_p is the phenomenological amplitude obtained from phase-shift analyses and M_c is the amplitude calculated using Eqs. (13)–(17). The chi-squared minimization with this weighting clearly emphasizes angular regions in which M_p is largest. This is not unreasonable since the amplitudes in

these regions are typically the best determined ones from the N-N data. Alternative weightings were tried but did not result in any systematic improvement in the quality of the fits. Below 425 MeV the tensor parts of the interaction were adequately represented by the same scheme. For higher energies, however, the tensor amplitudes possess too much structure for a satisfactory fit over the full angular range using this method. A compromise procedure, guided by the anticipated range of momentum transfers over which measurements of nucleon-nucleus scattering are most likely to be made, was adopted. In particular, those amplitudes in the region of momentum transfers between q_1 and q_2 were excluded from the evaluation of χ^2. The values of q_1, q_2, and the maximum allowable momentum transfer $q_{\max}$ in the N-N system are listed in Table II for the relevant energies.

The momentum transfers $q_2 < q < q_{\max}$ are important for calculating the knock-on exchange terms even for small momentum transfers in the nucleon-nucleus system as is implied in Eq. (10), and were therefore included in the calculation of χ^2.

B. Results

The complex effective interaction strengths (in the N-N system) which were obtained from the above search procedure are given in Table III for each bombarding energy considered. The maximum number of ranges in each N-N channel has been limited to no more than four for each of the central, spin-orbit, and tensor parts of the interaction.

The strengths in Table III which define t_{NN} require an A-dependent kinematic modification (renormalization) at each bombarding energy for calculating nucleon-nucleus scattering. This modification is provided by the transformation[4] of the t matrices given by

$$t_{NA} = \frac{\epsilon_0^2}{\epsilon_p \epsilon_t} t_{NN} \ , \tag{19a}$$

TABLE II. Values of q_1, q_2, and the maximum allowable momentum transfer $q_{\max}$ in the N-N system.

E_P (MeV)	q_1 (fm^{-1})	q_2 (fm^{-1})	$q_{\max}$ (fm^{-1})
425	3.10	4.50	4.53
515	3.10	4.90	4.98
650	3.50	5.50	5.60
800	4.00	6.18	6.21

where ϵ_p (ϵ_t) is the total energy of the incident (target) nucleon in the N-A system, ϵ_0 is the total energy of the incident nucleon in the N-N system, and t_{NA} is the interaction appropriate for N-A collisions. The energies in Eq. (19a) may readily be found using[13]

$$\epsilon_0^2 = m^2(1+\alpha), \ \epsilon_p^2 = m^2 + k_A^2 \ , \tag{19b}$$

$$\epsilon_t^2 = m^2 + (k_A/A)^2 \ ,$$

where

$$k_A^2 = m^2 A\beta \left[\frac{1+\alpha}{1+\beta} \right], \ \alpha \equiv \frac{E_P}{2m}, \ \beta \equiv \frac{4\alpha A}{(A+1)^2} \ . \tag{19c}$$

Here m is the mass of the proton, A is the nucleon number of the target, and E_P is the *kinetic* energy of the projectile in the laboratory system. In Eqs. (19), $\hbar = c = 1$.

In all of the calculations reported here both direct and knock-on exchange terms are included explicitly. In the plots of the t matrix the exchange terms were calculated in a well established short-range approximation[1] described in the Appendix. For nucleon-nucleus scattering the transition amplitudes for the exchange terms arising from the central and spin-orbit parts of the force may in this approximation be calculated using a *single* Yukawa of very short range (R_s) with strengths given by

$$V_x^C = \frac{\tilde{V}_x^C(k_A)}{4\pi R_s^3} \ \text{(central)} \ , \tag{20a}$$

$$V_x^{LS} = \frac{\tilde{V}_x^{LS}(k_A)/k_A}{8\pi R_s^5} \ \text{(spin-orbit)} \ , \tag{20b}$$

where k_A is the momentum of the incident nucleon in the NA system and $\tilde{V}^C(k_A)$ and $\tilde{V}^{LS}(k_A)$ are given by Eqs. (15). The subscript x indicates that the sign of the odd (even) state parts of the force for the central (spin-orbit) parts of the interaction are to be changed[2] for the exchange terms [see Eq. (A6)]. In the code DWBA70 (Ref. 14) one inputs

$$R_s = 0, \ V_x^C = \tilde{V}_x^C(k_A), \ V_x^{LS} = \tilde{V}_x^{LS}(k_A)/8\pi k_A \ . \tag{20c}$$

Although Table III contains the primary results of this work, the arrays of numbers provide little insight into the physical characteristics of V_{12} which are most important for nucleon-nucleus scattering.

TABLE III. Nucleon-nucleon t-matrix interaction strengths in the nucleon-nucleon c.m. system. The *TNE* and *TNO* strengths are in MEV fm^{-2}; all other are in MeV. The ranges are in fm. $NE \pm n$ denotes $N \times 10^{\pm n}$.

Real t-matrix interaction strengths at 100 MeV

Range	*SE*	*TE*	*SO*	*TO*
0.25	9.5413E + 03	1.1826E + 04	−2.0868E + 04	2.1482E + 04
0.40	−2.9111E + 03	−3.6366E + 03	2.9212E + 03	−3.4334E + 03
1.40	−1.0500E + 01	−1.0555E + 01	3.1500E + 01	3.5000E + 00

Range	*LSE*	*LSO*	*TNE*	*TNO*
0.25	−4.8470E + 03	−1.1177E + 03	5.1190E + 04	1.0766E + 03
0.40	−7.4436E + 02	−6.7802E + 02	−7.6871E + 03	3.1616E + 02
0.55			1.2272E + 03	−9.2075E + 01
0.70			−1.8828E + 02	3.6052E + 01

Real t-matrix interaction strengths at 140 MeV

Range	*SE*	*TE*	*SO*	*TO*
0.25	8.6245E + 03	7.3291E + 03	−2.1284E + 03	1.5686E + 04
0.40	−2.6731E + 03	−2.3762E + 03	7.7779E + 02	−2.6876E + 03
1.40	−1.0500E + 01	−1.0500E + 01	3.1500E + 01	3.5000E + 00

Range	*LSE*	*LSO*	*TNE*	*TNO*
0.25	−4.9122E + 03	−1.9861E + 03	3.0086E + 04	7.2020E + 02
0.40	−5.7205E + 02	−5.4126E + 02	−5.6510E + 03	2.9649E + 02
0.55			1.0120E + 03	−8.0624E + 01
0.70			−1.7234E + 02	3.3975E + 01

Real t-matrix interaction strengths at 210 MeV

Range	*SE*	*TE*	*SO*	*TO*
0.25	8.3428E + 03	6.8896E + 03	2.8694E + 04	6.1540E + 03
0.40	−2.5898E + 03	−2.2625E + 03	−4.1671E + 03	−1.2217E + 03
1.40	−1.0500E + 01	−1.0500E + 01	3.1500E + 01	3.5000E + 00

Range	*LSE*	*LSO*	*TNE*	*TNO*
0.15			5.9011E + 05	−5.6612E + 04
0.25	1.8237E + 04	−3.0309E + 03	−4.6759E + 04	6.2289E + 03
0.40	−2.2220E + 03	−3.4734E + 02	1.5392E + 03	−2.4544E + 02
0.55				
0.70			−7.7254E + 01	2.3683E + 01

Real t-matrix interaction strengths at 325 MeV

Range	*SE*	*TE*	*SO*	*TO*
0.25	9.4893E + 03	−2.2349E + 03	2.3285E + 03	6.3299E + 02
0.40	−3.6519E + 03	2.0882E + 03	1.0345E + 03	7.6312E + 02
0.55	3.2769E + 02	−6.4568E + 02	−3.1120E + 02	−3.5290E + 02
1.40	−1.0500E + 01	−1.0500E + 01	3.1500E + 01	3.5000E + 00

Range	*LSE*	*LSO*	*TNE*	*TNO*
0.15			9.2905E + 04	−3.0224E + 04
0.25	−9.5549E + 03	−2.2557E + 03	−1.1565E + 04	4.0423E + 03
0.40	7.3102E + 02	−4.4819E + 02	1.9614E + 02	−1.8458E + 02
0.55	−6.1560E + 01	3.6017E + 01		
0.70			−5.8213E + 01	2.2625E + 01

TABLE III. *(Continued).*

Imaginary t-matrix interaction strengths at 100 MeV

Range	*SE*	*TE*	*SO*	*TO*
0.25	$4.7123E+02$	$1.1116E+04$	$7.2863E+03$	$2.0492E+03$
0.40	$-2.9642E+02$	$-3.5628E+03$	$-1.4162E+03$	$-6.5360E+02$

Range	*LSE*	*LSO*	*TNE*	*TNO*
0.25	$-2.1203E+04$	$-1.1103E+03$	$1.5938E+04$	$-8.0323E+03$
0.40	$2.2050E+03$	$2.0844E+02$	$-2.5194E+03$	$1.0701E+03$
0.55			$3.3940E+02$	$-1.4792E+02$
0.70			$-2.8796E+01$	$1.3492E+01$

Imaginary t-matrix interaction strengths at 140 MeV

Range	*SE*	*TE*	*SO*	*TO*
0.25	$9.3847E+02$	$9.7881E+03$	$2.3836E+03$	$3.1138E+02$
0.40	$-3.5470E+02$	$-3.1290E+03$	$-9.5286E+02$	$-4.3188E+02$

Range	*LSE*	*LSO*	*TNE*	*TNO*
0.25	$-7.0973E+03$	$-6.5588E+02$	$1.3842E+04$	$-8.4506E+03$
0.40	$1.2683E+03$	$1.1842E+02$	$-2.5772E+03$	$1.3076E+03$
0.55			$4.2067E+02$	$-2.1472E+02$
0.70			$-4.1723E+01$	$2.2136E+01$

Imaginary t-matrix interaction strengths at 210 MeV

Range	*SE*	*TE*	*SO*	*TO*
0.25	$1.4554E+03$	$9.3304E+03$	$-3.6458E+03$	$-1.3619E+03$
0.40	$-4.6702E+02$	$-3.0314E+03$	$-5.7032E+01$	$-1.6364E+02$

Range	*LSE*	*LSO*	*TNE*	*TNO*
0.15			$4.3777E+05$	$-1.3450E+05$
0.25	$1.6095E+03$	$-7.5471E+01$	$-3.2667E+04$	$8.4506E+03$
0.40	$5.3886E+02$	$2.9356E+01$	$9.9377E+02$	$-2.7481E+02$
0.70			$-9.8710E+00$	$3.0775E+00$

Imaginary t-matrix interaction strengths at 325 MeV

Range	*SE*	*TE*	*SO*	*TO*
0.25	$2.3372E+03$	$5.6348E+03$	$-7.8145E+03$	$-3.2250E+03$
0.40	$-1.0523E+03$	$-1.8533E+03$	$9.1721E+02$	$3.5309E+02$
0.55	$1.2506E+02$	$-3.7852E+01$	$-1.5548E+02$	$-6.2928E+01$

Range	*LSE*	*LSO*	*TNE*	*TNO*
0.15			$9.3881E+04$	$-8.1725E+04$
0.25	$5.0687E+03$	$1.2226E+03$	$-7.3845E+03$	$5.7850E+03$
0.40	$-1.4201E+02$	$-1.7649E+02$	$2.6879E+02$	$-2.4220E+02$
0.55	$3.9740E+01$	$2.0141E+01$		
0.70			$-3.8720E+00$	$3.6473E+00$

TABLE III. *(Continued).*

Real t-matrix interaction strengths at 425 MeV

Range	*SE*	*TE*	*SO*	*TO*
0.25	6.8287*E* + 03	5.8852*E* + 03	1.8599*E* + 02	2.7073*E* + 03
0.40	−2.2126*E* + 03	−3.2752*E* + 03	1.6471*E* + 03	−1.0842*E* + 02
0.55	3.6141*E* + 01	7.2025*E* + 02	−4.4038*E* + 02	−1.7964*E* + 02
1.40	−1.0500*E* + 01	−1.0500*E* + 01	3.1500*E* + 01	3.5000*E* + 00

Range	*LSE*	*LSO*	*TNE*	*TNO*
0.15			−4.0147*E* + 04	−3.5474*E* + 04
0.25	−3.1947*E* + 03	−2.6013*E* + 03	−1.6954*E* + 02	3.9896*E* + 03
0.40	2.6781*E* + 01	−2.4963*E* + 02	−2.2943*E* + 02	−1.7476*E* + 02
0.55	−7.1692*E* + 00	2.3428*E* + 01		
0.70			−5.3228*E* + 01	2.1063*E* + 01

Real t-matrix interaction strengths at 515 MeV

Range	*SE*	*TE*	*SO*	*TO*
0.25	5.7228*E* + 03	3.0728*E* + 03	−7.5714*E* + 03	4.5532*E* + 03
0.40	−1.8439*E* + 03	−1.7333*E* + 03	4.0373*E* + 03	−8.2334*E* + 02
0.55	2.1671*E* + 01	4.5172*E* + 02	−7.8909*E* + 02	−5.7015*E* + 01
1.40	−1.0500*E* + 01	−1.0500*E* + 01	3.1500*E* + 01	3.5000*E* + 00

Range	*LSE*	*LSO*	*TNE*	*TNO*
0.11			−1.8644*E* + 06	−3.7231*E* + 05
0.15			3.9510*E* + 05	7.9906*E* + 04
0.25	−4.2488*E* + 02	−2.6705*E* + 03	−1.1271*E* + 04	−1.3484*E* + 03
0.40	−3.5647*E* + 02	−1.3253*E* + 02		
0.55	3.1533*e* + 01	1.3676*E* + 01		
0.70			−5.3066*E* + 01	1.8300*E* + 01

Real t-matrix interaction strengths at 650 MeV

Range	*SE*	*TE*	*SO*	*TO*
0.15	−2.4085*E* + 03	−1.0714*E* + 04	2.5964*E* + 05	−1.1978*E* + 05
0.25	4.2161*E* + 03	4.5508*E* + 03	−5.3371*E* + 04	2.9138*E* + 04
0.40	−1.0608*E* + 03	−2.6296*E* + 02	3.8919*E* + 03	−2.6525*E* + 03
1.40	−1.0500*E* + 01	−1.0500*E* + 01	3.1500*E* + 01	3.5000*E* + 00

Range	*LSE*	*LSO*	*TNE*	*TNO*
0.11			−2.3411*E* + 06	−8.1288*E* + 05
0.15	6.3296*E* + 04	6.1049*E* + 03	5.4106*E* + 05	2.0930*E* + 05
0.25	−7.3926*E* + 03	−2.9713*E* + 03	−1.5923*E* + 04	−6.0900*E* + 03
0.40	1.3889*E* + 02	−8.2300*E* + 01		
0.70			−4.9939*E* + 01	1.8967*E* + 01

Real t-matrix interaction strengths at 800 MeV

Range	*SE*	*TE*	*SO*	*TO*
0.15	−1.5967*E* + 04	−2.0450*E* + 04	2.7015*E* + 05	−1.0959*E* + 05
0.25	9.1306*E* + 03	8.3590*E* + 03	−6.0416*E* + 04	2.7122*E* + 04
0.40	−1.3824*E* + 03	−6.0888*E* + 02	4.7533*E* + 03	−2.3920*E* + 03
1.40	−1.0500*E* + 01	−1.0500*E* + 01	3.1500*E* + 01	3.5000*E* + 00

Range	*LSE*	*LSO*	*TNE*	*TNO*
0.11			−2.2484*E* + 06	−7.4613*E* + 05
0.15	3.8542*E* + 04	6.7866*E* + 03	5.2942*E* + 05	1.9727*E* + 05
0.25	−5.5550*E* + 03	−2.1624*E* + 03	−1.5420*E* + 04	−5.0162*E* + 03
0.40	1.4001*E* + 02	−1.4352*E* + 02		
0.70			−4.6868*E* + 01	1.7324*E* + 01

TABLE III. *(Continued).*

Imaginary t-matrix interaction strengths at 425 MeV

Range	*SE*	*TE*	*SO*	*TO*
0.25	2.5202E + 03	3.1695E + 03	−7.6590E + 03	−3.1683E + 03
0.40	−1.2429E + 03	−9.8963E + 02	1.0011E + 03	3.3104E + 02
0.55	1.5035E + 02	−8.0551E + 01	−1.6170E + 02	−6.0174E + 01

Range	*LSE*	*LSO*	*TNE*	*TNO*
0.15			6.7339E + 04	−6.1820E + 04
0.25	2.3320E + 03	1.5541E + 03	−5.4310E + 03	4.2059E + 03
0.40	−3.7560E + 01	−2.2744E + 02	2.4755E + 02	−1.6390E + 02
0.55	2.5329E + 01	2.6157E + 01		
0.70			−2.9019E + 00	2.2275E + 00

Imaginary t-matrix interaction strengths at 515 MeV

Range	*SE*	*TE*	*SO*	*TO*
0.25	4.2504E + 03	1.9390E + 03	−4.4010E + 03	−3.0858E + 03
0.40	−2.1835E + 03	−5.0129E + 02	4.1544E + 02	2.5121E + 02
0.55	2.9634E + 02	−1.3730E + 02	−9.1172E + 01	−5.2693E + 01

Range	*LSE*	*LSO*	*TNE*	*TNO*
0.11			3.2957E + 05	−3.9512E + 05
0.15			−4.8213E + 04	5.5146E + 04
0.25	1.4438E + 03	2.1867E + 03	1.1377E + 03	−5.0251E + 02
0.40	5.2301E + 01	−3.2854E + 02		
0.55	1.2091E + 01	3.8551E + 01		
0.70			−5.2653E − 02	2.3782E − 01

Imaginary t-matrix interaction strengths at 650 MeV

Range	*SE*	*TE*	*SO*	*TO*
0.15	1.6482E + 04	−1.2669E + 04	−8.2784E + 04	−1.9094E + 04
0.25	−4.0309E + 03	7.6182E + 03	1.4633E + 04	3.2804E + 03
0.40	−4.7445E + 02	−1.5539E + 03	−1.2282E + 03	−7.4353E + 02

Range	*LSE*	*LSO*	*TNE*	*TNO*
0.11			−1.9574E + 05	−6.4302E + 05
0.15	2.0647E + 03	3.2633E + 03	7.9456E + 04	1.3311E + 05
0.25	9.0278E + 02	8.6545E + 02	−1.1906E + 03	−3.0501E + 03
0.40	1.1690E + 02	−2.0265E + 00		
0.70			4.1314E − 01	4.4476E − 01

Imaginary t-matrix interaction strengths at 800 MeV

Range	*SE*	*TE*	*SO*	*TO*
0.15	1.5442E + 04	−8.1596E + 03	−9.4213E + 04	5.9214E + 03
0.25	−4.7467E + 03	5.3973E + 03	1.7999E + 04	−1.3338E + 00
0.40	−2.8861E + 02	−1.2020E + 03	−1.5598E + 03	−9.4798E + 02

Range	*LSE*	*LSO*	*TNE*	*TNO*
0.11			−3.5747E + 05	−9.6022E + 05
0.15	1.2851E + 04	−3.5958E + 03	1.2896E + 05	2.3355E + 05
0.25	−9.1877E + 01	2.0807E + 03	−2.6253E + 03	−7.0829E + 03
0.40	9.4667E + 01	−4.6092E + 01		
0.70			1.2528E + 00	2.5695E + 00

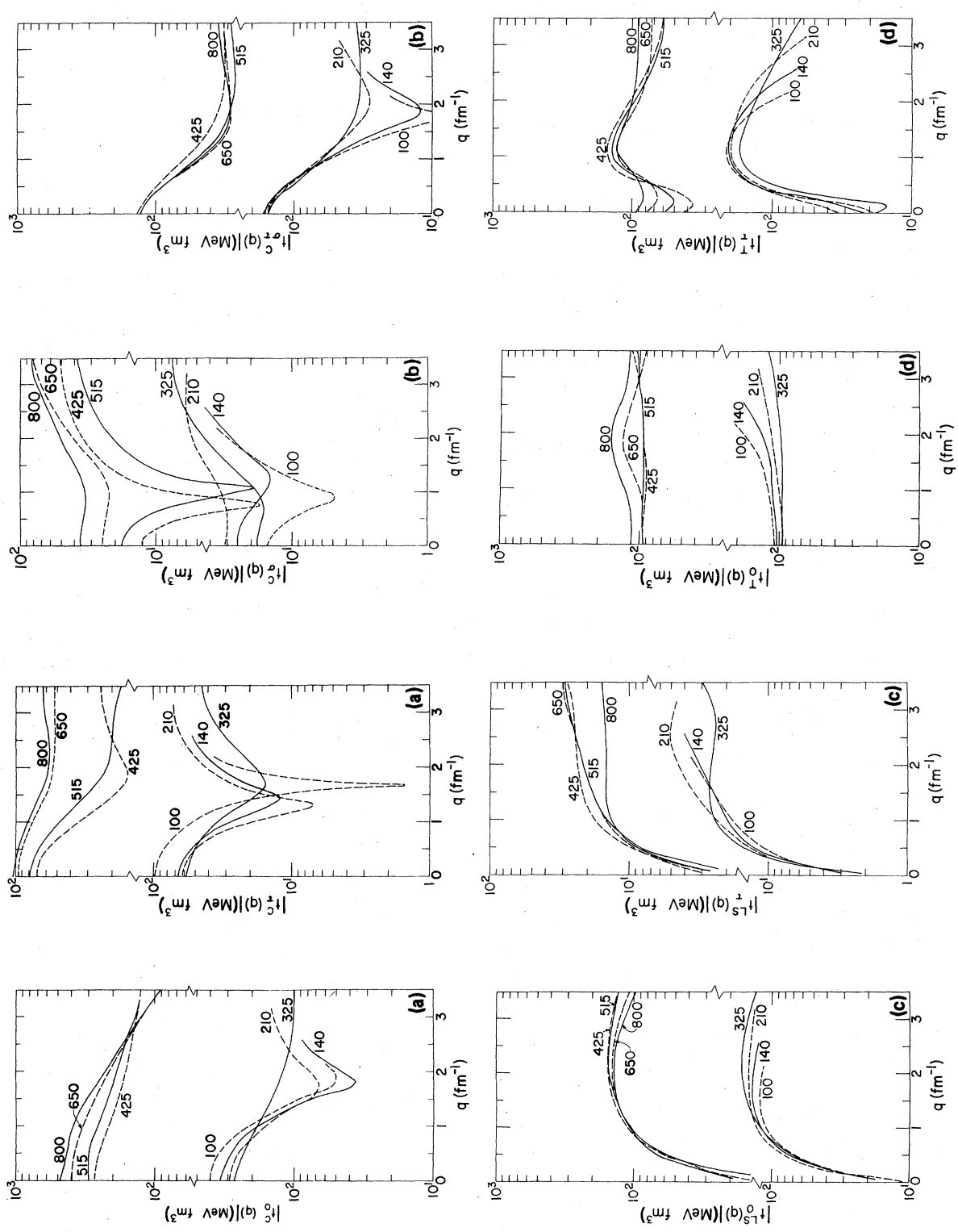

FIG. 1. Magnitudes of the spin and isospin transfer components (direct + exchange) of the N-N interaction as a function of bombarding energy in MeV (number on curve) and momentum transfer. See the Appendix and Eq. (16) for details. The momentum in the nucleon-nucleus system was calculated using $A = 28$ which yields an average value of k_A for typical targets. The factor $(2 + \xi)^{\frac{1}{2}}$ is not included in t_σ^C or $t_{\sigma\tau}^C$.

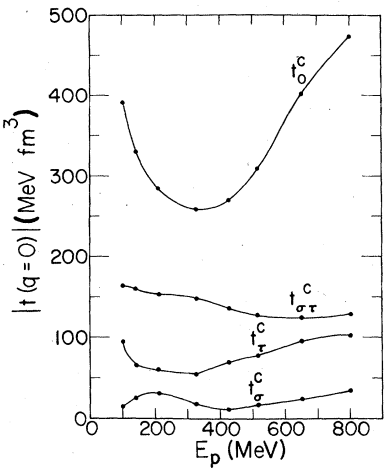

FIG. 2. Energy dependence of the magnitude of the central parts of the N-N t matrix as described in Fig. 1.

To illustrate the roles of the various parts of V (or t) in nuclear excitations, we have formed the moduli of the components of the t matrix as they enter (direct + exchange) into the evaluation of nucleon-nucleus cross sections. The details are presented in the Appendix, where it is shown that for natural parity excitations, $|t^{LS}|$ and the non-spin-transfer part of $|t^C|$ represent the appropriate strengths; for unnatural parity excitations the relevant strengths are $|t^{LS}|$, $(2+\xi)^{1/2}|t_\sigma^C|$, and $|t^T|$ for the spin-orbit, central, and tensor terms, respectively. In the Appendix, these t's are related to those in Eq. (16); here we simply note that ξ is dependent on nuclear structure and t_σ^C corresponds to the spin-transfer component of t^C.

Figure 1 shows a plot of each of these parts of t as a function of both momentum transfer and bombarding energy and in a rough way represents a map of the probe characteristics at intermediate energies. A number of rather general observations can be made from Fig. 1.

Although strongly energy dependent, the scalar-isoscalar part of the N-N interaction (t_0^C) dominates at all of the energies considered, particularly for momentum transfers $q \lesssim 1$ fm^{-1}. Above ~ 400 MeV, t_0^C dominates out to $q \gtrsim 2$ fm^{-1}. The dominance of t_0^C and its energy dependence are illustrated more clearly in Fig. 2, where the magnitudes of the central parts of the t matrix are plotted at $q = 0$ as a function of bombarding energy. A similar plot at $q = 1$ fm^{-1} exhibits the same qualitative features. As a result, the small-q part of the nucleon-nucleus excitation spectrum should typically be dominated by scalar-isoscalar modes of excitation, especially above $E_P = 400$ MeV. Because of the weakness (or absence) of low-lying 0^+ and 1^- isoscalar states in nuclei, the excitation of 1^+ states at very small q in parts of the excitation spectrum is a notable exception. For larger momentum transfers t_0^{LS} becomes important for isoscalar excitations of natural parity, especially for high-spin states below $E_P = 400$ MeV. As can be seen in Fig. 2, t_τ^{LS} is small and should be relatively unimportant for the excitation of natural parity states at all of the energies considered. When analyzing powers are considered, t_0^{LS} and t_τ^{LS} can of course be relatively more important.

With the exception of large q, t_σ^C is relatively weak (and poorly determined) at all bombarding energies. The strong isoscalar part of t^{LS} is nearly energy independent as is the isoscalar part of t^T which, dominated by the knock-on exchange terms, is also nearly independent of q. Of the central parts of the force, $t_{\sigma\tau}^C$ changes least with bombarding energy. This stability is most likely derived from the energy independent OPEP that dominates this part of the interaction. Similarly, the isovector part of the tensor force changes slowly with energy. Its strength is larger than but comparable to t_o^T.

The excitation of isovector unnatural parity states should be dominated by $t_{\sigma\tau}^C$ at small q ($q \lesssim 1$ fm^{-1}); for larger q, t_τ^T should dominate. For isoscalar unnatural parity excitations there is considerable competition amongst t_σ^C, t_0^{LS}, and t_0^T for $q \gtrsim 1$ fm^{-1}; for smaller, q, t_0^T dominates (through the knock-on exchange terms), especially below 200 MeV.

The interaction has some especially interesting implications when we isolate its isovector components as is done[15] experimentally in the (p,n) reaction. Figure 3 shows a plot of $|t_{\sigma\tau}^C/t_\tau^C|^2$ at

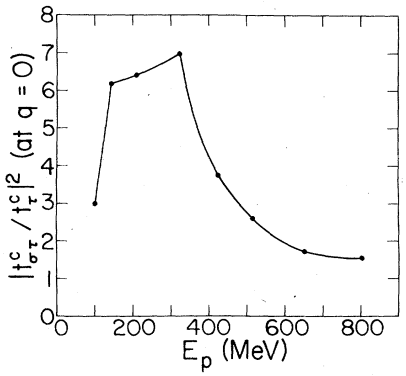

FIG. 3. Energy dependence of the ratio $|t_{\sigma\tau}^C/t_\tau^C|^2$ at zero momentum transfer.

$q = 0$ as a function of bombarding energy. Apart from the nuclear matrix element, this ratio indicates the relative sensitivity of the (p,n) reaction near $q = 0$ to spin-flip versus non-spin-flip modes of excitation. The dramatic peak in this ratio between ~ 100- and 350-MeV bombarding energy provides a window for looking at isovector spin-flip modes, a task much more difficult at lower energies where $t_{\sigma\tau}^C \sim t_\tau^C$. The strong energy dependence of this ratio has already proven especially important for interpreting recent (p,n) results between 100 and 200 MeV where significant amounts of Gamow-Teller strength ($\Delta S = 1 = \Delta T$) have been identified.[16] Qualitatively similar results hold for $q \simeq 1$ fm^{-1}, which suggest a more general enrichment of $\Delta S = 1$ excitations in (p,n) spectra at these energies. Indeed $\Delta S = 1$ modes of higher multipolarity ($L = 1$) have been identified.[16] Figure 4 shows a plot of the ratio of $|t_{\sigma\tau}^C/t_\tau^C|^2$ as a function of q for $E_P = 140$ and 210 MeV. This ratio becomes extremely large for $1 \lesssim q(\text{fm}^{-1}) \lesssim 1.5$, where t_τ^C is very small, suggesting that the (p,n) spectrum should be nearly void of $\Delta S = 0$ modes near these momentum transfers. The inclusion of the tensor force should make this argument even stronger, suggesting that isovector modes of moderately high spin might be identified in this region of momentum transfer.

In addition to their magnitudes, the relative phases of the various parts of the t matrix play an important role in interpreting nucleon-nucleus scattering, especially when measurements of spin observables are considered. This is especially evident in the plane-wave impulse approximation (PWIA) (assuming no energy loss) where the analyzing power is, in the present notation, given by[4]

$$A_y(q) = \frac{2(t_R^{LS} t_I^C - t_I^{LS} t_R^C)}{|t^C|^2 + |t^{LS}|^2}, \quad \Delta S = 0 \tag{21a}$$

for natural parity transitions. For unnatural parity transitions, the corresponding result is given by[4]

$$A_y(q) = \frac{2[t_R^{LS}(t_I^C + t_I^{T\beta}) - t_I^{LS}(t_R^C + t_R^{T\beta})]}{|t_{LS}|^2 + |t^C + t^{T\alpha}|^2 + |t^C + t^{T\beta}|^2 + \xi|t^C + t^{T\gamma}|^2} . \tag{21b}$$

Here t_R (t_I) denotes the real (imaginary) part of t; the appropriate isospin combination must be taken, and t^C in Eq. (21a) [Eq. (21b)] is the non-spin-transfer (spin-transfer) component of t^C. The α, β, and γ parts of t^T are defined in the Appendix.

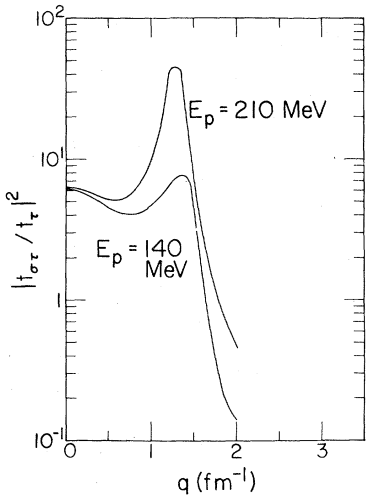

FIG. 4. Momentum transfer dependence of the ratio $|t_{\sigma\tau}^C/t_\tau^C|^2$ at 140 and 210 MeV.

Although optical model distortion effects should be included in any quantitative comparison of IA calculations with experiment, Eqs. (21a) and (21b) have proven helpful[17,18] in understanding some of the *qualitative* aspects of analyzing powers (A_y) in terms of the magnitude and phase of the N-N force. This is especially true when A_y is moderately large in the PWIA; for those transitions in which the PWIA estimate is small, distortion effects typically play a major role. Figure 5 illustrates some of the anticipated trends in A_y at a few selected energies based on the present t matrix (see the Appendix).

For isoscalar transitions of natural parity, the A_y in the PWIA are characterized by moderately large and positive values especially at small q. This overall trend is borne out by both DWIA calculations and experimental data[17] for such transitions. This feature arises from the large negative values of both t_I^C and t_R^{LS} which tend to dominate the central and spin-orbit parts of the t matrix at intermediate energies. The node in $A_y(q)$ near $q = 2$ fm^{-1} arises primarily from a node in t_I^C; DWIA calculations and measurements of A_y on light nuclei below $E_P = 200$ MeV confirm the existence[17] of such a node.

For isovector transitions having natural parity

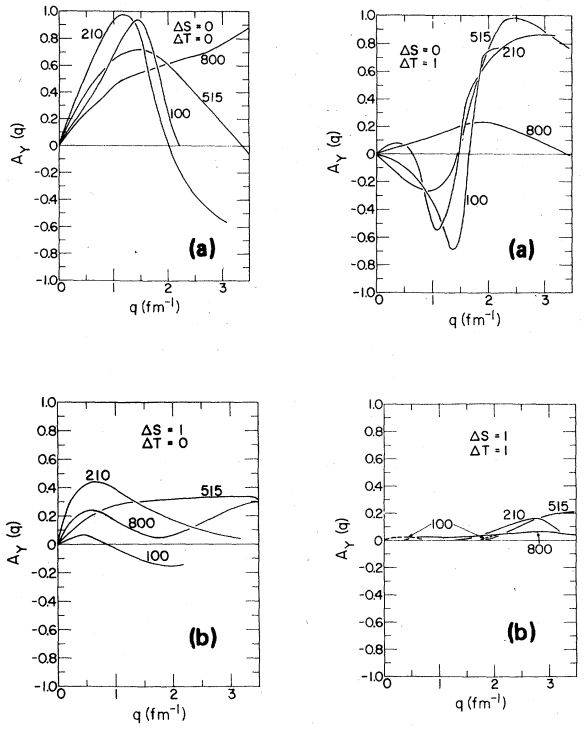

FIG. 5. PWIA estimates of nucleon-nucleus analyzing powers as a function of bombarding energy, momentum transfer, and spin and isospin transfer. See the Appendix for some of the limitations on these rough estimates.

($\Delta S = 0$); the sign of A_y at small q (for energies below ~ 800 MeV) is opposite that for isoscalar transitions and this suggests an important signature for distinguishing between these types of excitations. Because of the much greater strength of the $\Delta T = 0$ part of the t matrix, A_y for those transitions involving an appreciable $\Delta T = 0$ component should tend to look more like the $\Delta T = 0$ curve. It has been suggested[17] that this isospin dependence might be used as a probe of the neutron-proton composition of transition densities, especially when the corresponding (e,e') data are available for comparison.

For isovector excitations of unnatural parity ($\Delta S = 1$) the PWIA predictions yield very small analyzing powers. This may be traced to the small isovector component of t^{LS}, especially its imaginary part, and the predominantly real $t^C_{\sigma\tau}$ and t^T_τ. Near $E_P = 800$ MeV the experimental A_y are observed[18] to be quite small; between 100 and 200 MeV, A_y for this class of transitions is not uniformly small, but this has been shown[17] to arise largely from the optical model spin-orbit potential, particularly at small q.

For isoscalar transitions of unnatural parity, A_y is predicted to be moderately large at some energies but small at others; in practice, these simple estimates of A_y for this class of transitions tend to be rather unreliable. Although the isoscalar part of t^{LS} is reasonably well determined, t^C_σ is not. Moreover, it is implicit in our simple estimates of A_y that the polarization $P = A_y$ and this is often not even qualitatively true. This arises from the large contribution to this type of transition from the amplitudes E and F in Eq. (2) which have been shown[19] to be responsible for differences between P and A_y even in the absence of optical-model spin-orbit distortion. A residuum[17] of the PWIA results has nevertheless been noted in a few transitions of this type.

C. Uncertainties in t

Although a systematic study of the errors and uncertainties leading to the effective interaction would be desirable, this is an unwieldy task beyond the intent of this work and is made impractical by the theoretical model used. Nevertheless, it is convenient to separate the uncertainties in V_{12} into two categories: (1) those uncertainties in the "experimental" amplitudes [Eq. (2)] used to construct V_{12}; and (2) those uncertainties which arise from representing the amplitudes by a local operator as in Eq. (12).

A moderately complete discussion of errors in this first category is given in Ref. 10, where the phase shifts are presented (also see Ref. 12). Typically, the errors in the largest phase shifts are $\pm 5\%$ or smaller; errors in the mixing parameter $\bar{\epsilon}_1$ tend to be larger, $\sim \pm 10\%$. On the average, the amplitudes cannot be regarded as known any better than $\pm(5-10\,\%)$. Near 800 MeV the uncertainties are larger[12] due to the scarcity of $p + n$ data.

Uncertainties in representing the N-N t matrix arise not only from the ansatz of a local V_{12} but also from its parametric form. Even within the framework of a multiple-Yukawa representation and the constraint of an OPEP tail on V^C, there are ambiguities. These ambiguities take the form of acceptable (usually excellent) and nearly equivalent fits to the on-shell N-N amplitudes, leading to somewhat different results for $t(E,q)$ for nucleon-nucleus scattering. The source of difficulty can be illustrated using Eqs. (9) and (10), where $\tilde{V}(q)$ may differ for two different fits with $\tilde{V}(Q)$ compensating for

this difference to yield essentially equivalent on-shell fits. In the nucleon-nucleus system, $\tilde{V}(q)$ remains the same for a given q, but $\tilde{V}(k_A)$ obtained from different fits to t_{NN} may not give equivalent values of the sums $\tilde{V}(q) + \tilde{V}(k_A)$. This argument holds when the exchange terms are calculated exactly; the use of $\tilde{V}(k_A)$ makes the argument more transparent. This source of uncertainty is most severe for the central parts of the interaction at large q, particularly at the lower bombarding energies.

Figure 6 shows $t^C_{\sigma\tau}$ at $E_P = 325$ MeV for four different fits to t_{NN} and illustrates the type of uncertainties which can be expected. Similar results for the other parts of t^C suggest that t^C should be moderately reliable out to $q \sim 1.0$ fm^{-1} at $E_P = 100$ MeV. The greater importance of t^{LS} and t^T at larger q tends to extend the validity of our representation of t to larger q but this is not always assured. We have attempted to reduce this type of ambiguity by choosing ranges which do not result in excessive cancellation between $V(q)$ and $V(k_A)$; this was not always possible. Clearly, more work on removing this ambiguity is needed. This might necessitate the use of an N-N potential model.

III. SELECTED APPLICATIONS OF THE EFFECTIVE INTERACTION

In this section we show a few applications of V_{12} in the DWIA approximation. It is not the purpose here to provide a thorough interpretation or analysis of the experimental data shown, but rather to get a feel for how well (or poorly) this version of the DWIA works and in addition illustrate some of the points discussed in Sec. II B. The specific applications are separated according to the incident energy (E_P) in the lab system since the detailed validity of the DWIA is closely linked to E_P and, as discussed in Sec. II, the characteristics of the effective interaction are expected to change with bombarding energy.

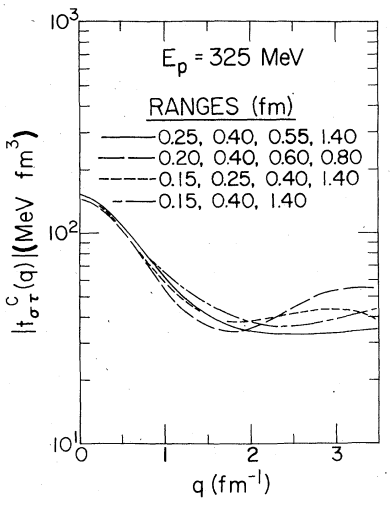

FIG. 6. An illustration of some of the uncertainties incurred in representing the $t^C_{\sigma\tau}$ component of the N-N t matrix in the present model with different choices of ranges.

For the calculations reported here, the short-range approximation [Eq. (20c)] for the central and spin-orbit parts of the force has been used for the natural parity excitations and for the 6^- transitions in ^{28}Si for $E_P > 200$ MeV. Modified versions of the code DWBA70 (Ref. 14) were used and the exchange terms arising from the tensor force were included exactly. The distorted waves were chosen to fit elastic scattering.

A. Applications for $100 \lesssim E_P$ (MeV) $\lesssim 200$

Data for the cases we discuss in this section have been taken at the Indiana University Cyclotron Facility. The 140 MeV t matrix was used.

1. The ^{12}C(p,p') reaction at 120 MeV

Transitions within the ^{12}C nucleus provide a rich sampling of several of the components of any effective interaction. Moreover, shell-model wave functions are available which reproduce many of the known properties of these transitions. Here we compare DWIA calculations using the present interaction with recent cross section data[20] for transitions to the 1^+ states at 12.7 ($T = 0$) and 15.1 ($T = 1$) MeV and to the 2^+ states at 4.44 ($T = 0$) and 16.1 ($T = 1$) MeV. The results using Cohen-Kurath[21] wave functions (CKWF), (8 – 16) POT as a starting point are shown in Fig. 7. The optical model parameters are taken from Ref. 20 and the CKWF have been modified as described below. These transitions are discussed in more detail in Ref. 20.

For the 2^+ state at 4.44 MeV, the CKWF reproduce the shape of the longitudinal (e,e') form factor[22] out to $q \sim 2$ fm^{-1} but underestimate its magnitude by a factor of 2. When this renormalization is included the calculated (p,p') cross section (which is sensitive to t^C_0 and t^{LS}_0) is too large by a factor of ~ 1.7 near the first maximum; for $q \sim 1.4$

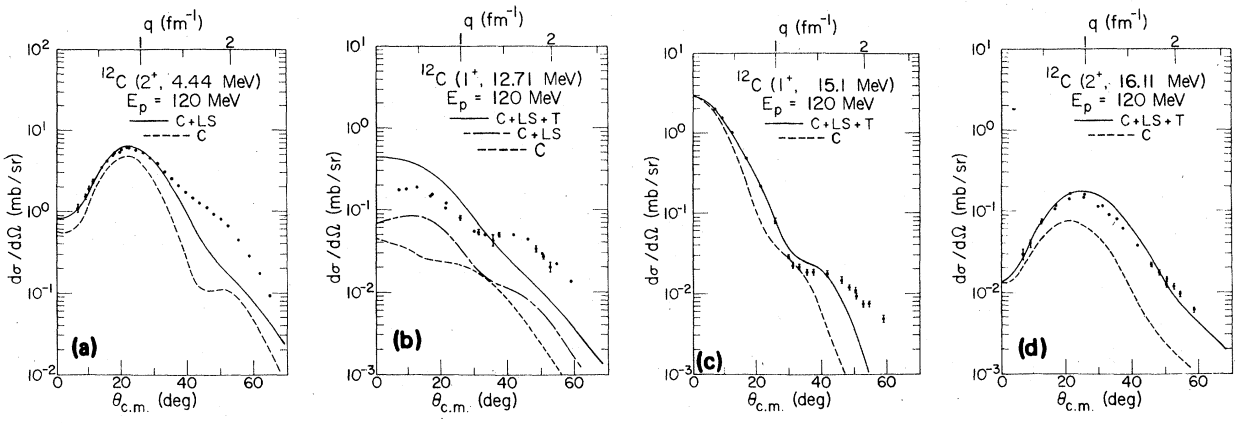

FIG. 7. A comparison between DWIA calculations using the 140 MeV t matrix and experimental data for the excitation of p-shell states in ^{12}C at $E_P = 120$ MeV. The wave functions deviate from the CKWF as described in the text.

fm^{-1} the discrepancy is much smaller. The failure of the DWIA for $100 < E_P$ (MeV) 200 for transitions of this type ($\Delta S = 0 = \Delta T$) has been interpreted[9] in terms of Pauli corrections to nucleon-nucleon scattering in the presence of other nucleons and is not peculiar to this nucleus.

Excitation of the 2^+ $T = 1$ state at 16.1 MeV can proceed via t_τ^C, $t_{\sigma\tau}^C$, t_τ^{LS}, and t_τ^T; t_τ^{LS} is negligibly small. Since the CKWF yield comparable transition densities for $S = 0$ and 1 and at this bombarding energy $|t_{\sigma\tau}^C/t_\tau^C|^2 >> 1$, this excitation proceeds primarily by $t_{\sigma\tau}^C$ and t_τ^T. Inelastic electron scattering measurements of both longitudinal ($\Delta S = 0$) and transverse ($\Delta S = 1$) form factors for this transition have recently been made.[22] The corresponding CKWF transition densities have been renormalized separately to agree with these measurements and these renormalized densities were used in the calculations shown in Fig. 7. The agreement between theory and experiment is quite good over the full angular range where there is data. This transition is seen to be especially sensitive to the isovector part of the tensor force.

Excitation of the 1^+ $T = 0$ state at 12.7 MeV is mediated by t_σ^C, t_0^{LS}, and t_0^T. As noted earlier t_σ^C is weak; t_0^T is large because of the knock-on exchange terms. For this transition the (e,e') reaction has been of little help in calibrating the transition density due to its extreme sensitivity[22] to small isovector impurities. Therefore the calculations in Fig. 7 were done using the unmodified CKWF. The DWIA results are in rather poor agreement with the experimental data. Although the source of difficulty is not well understood, the discrepancy is largely removed at higher bombarding energies (see Sec. III B).

Excitation of the 1^+ $T = 1$ state at 15.1 MeV is mediated primarily by $t_{\sigma\tau}^C$, whose origin is largely the OPEP. The CKWF are known[20,22] from (e,e') and β-decay measurements to be quite good for $q \lesssim 1$ fm^{-1} ($\theta_{c.m.} \sim 25°$) and quite poor for larger q. Hence we can only test the t-matrix interaction for $q \lesssim 1$ fm^{-1}. A comparison of DWIA calculations with experimental data in Fig. 7 indicates the essential correctness of the strength of the $\Delta S = 1 = \Delta T$ part of the present t-matrix interaction for $q \lesssim 1$ fm^{-1}; t_τ^T is essential for $q > 0.3$ fm^{-1}.

2. *The $^{28}Si(p,p')$ reaction at 135 MeV*

In this nucleus we consider the excitation of the 6^- states at 11.58 MeV ($T = 0$) and 14.35 MeV ($T = 1$) and the 5^- state at 9.7 MeV ($T = 0$). Figure 8 shows a comparison between DWIA calculations and measured cross sections of Yen *et al.*[17] Each of the transition densities was assumed to arise from the $(f_{7/2},d_{5/2}^{-1})$ configuration. Harmonic oscillator wave functions were used with $b = 1.91$ fm (1.82 fm) for the 5^- (6^-) transitions.

The 5^- transition is dominated by t_0^{LS}. After the transition density is normalized to fit the longitudinal form factor deduced from (e,e') measurements,[23] the calculated cross section is too large by a factor of ~ 1.85; the calculated shape is in good agreement with the data. The overestimate of the cross section for this transition suggests that t_0^{LS} may be too large, especially since density-dependent corrections[9] are believed to be most important for

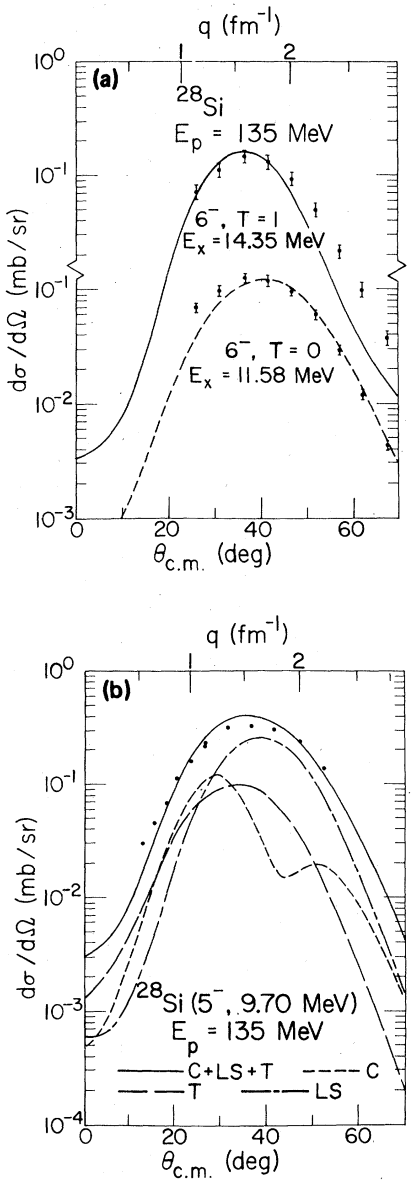

FIG. 8. Comparison between DWIA calculations (140 MeV t matrix) and measured cross sections at $E_P = 135$ MeV for exciting relatively high spin states of natural and unnatural parity in ^{28}Si. The normalizations of the transition densities used are discussed in the text.

t^C. A similar overestimate was noted for the isoscalar 2_1^+ cross section in ^{12}C.

The calculated DWIA cross section agrees reasonably well in shape with the experimental data for the 6^-, $T = 1$ transition. The magnitude of the calculated cross section is too large by roughly a factor of 4.8 when the transition is treated as a pure particle-hole excitation. The same transition density overestimates the corresponding (e,e') cross section[23] by a factor of ~ 3.3. Hence the calculated (p,p') cross section is too large relative to the (e,e') cross section by 40–50%. The central, spin-orbit, and tensor force contributions to the cross section are in the ratio 1.0:0.5:7.7, respectively. This result is in contrast to that for the 16.1 MeV $T = 1$ state in ^{12}C where the tensor force appears to be of the correct magnitude.

For the 6^-, $T = 0$ excitation (e,e') data are unavailable for calibrating the transition density. The shape of the calculated cross section is in excellent agreement with the data but the single particle-hole amplitude gives a cross section too large by a factor of ~ 11.0. This large an overestimate is not peculiar to the present interaction and is discussed in Ref. 17. The central, spin-orbit, and tensor contributions to the cross section are in the ratio 1.0:14:14.

The calculated analyzing powers for each of these three states are in poorer agreement with the data than those shown in Ref. 17. This is not understood since, in principle, the present interaction is more complete than that used in Ref. 17.

These transitions in ^{28}Si provide an interesting example of the energy dependence of the effective interaction. In particular, it has already been noted[24] that high-spin states of unnatural parity are much less prevalent in (p,p') spectra at 800 MeV compared with analogous spectra near 135 MeV. In Fig. 9 we show the ratios of the calculated peak cross sections for the 5^- and 6^- states between 100 and 800 MeV based on the pure particle-hole wave functions used above. In light of the comparison with experimental data above we focus only on the energy dependence of these ratios. The peak cross sections for these states occur at similar momentum transfers ($q \sim 1.5-1.7$ fm^{-1}) and their shapes

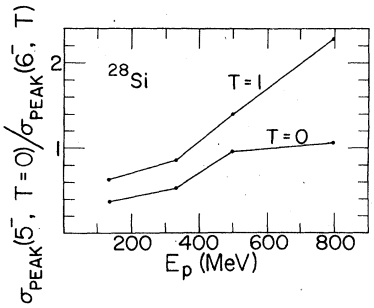

FIG. 9. Ratios of calculated peak cross sections for the 5^- and 6^- states in ^{28}Si between $E_P = 100$ and 800 MeV.

change slowly with energy when plotted against q. The relative size of the 5^- cross section is predicted to increase by a factor of ~ 3 (4) compared with the 6^-, $T = 0$ ($T = 1$) level. This increase is due to the large increase in t_0^C with increasing energy (see Fig. 2).

3. *The ^{90}Zr(p,n) reaction at 120 MeV*

We consider the (p,n) reaction to the isobaric analog of the ^{90}Zr ground state. This type of transition samples primarily the t_τ^C part of the effective interaction, especially at forward angles. Figure 10 shows a comparison of DWIA results with experimental data[16] for this transition. The DWIA calculations were made by assuming that the neutron excess may be described by the $(g_{9/2})^{10}$ configuration with an oscilllator length of 2.12 fm. Both the shape and the magnitude of the calculated differential cross section are in excellent agreement with the available data ($q \lesssim 0.65$ fm^{-1}). Preliminary estimates[25] suggest that Pauli corrections would reduce the calculated cross section at forward angles. This will be investigated elsewhere. It should be noted (see Fig. 3) that t_τ^C is changing especially rapidly in this energy range and that the 100 MeV interaction significantly overestimates this cross section. Moreover, at 120 MeV the knock-on exchange terms

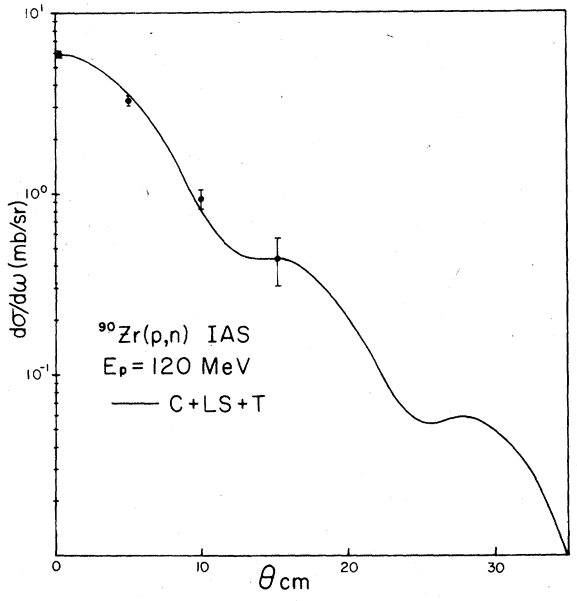

FIG. 10. Comparison of DWIA results with experimental data for excitation of the isobaric analog of the ^{90}Zr ground state at $E_P = 120$ MeV.

sample momentum transfers unavailable in the N-N system at 100 MeV.

B. Applications near $E_P = 400$ MeV

It has been noted[26] that the impulse approximation is not in quantitative agreement with either reaction or total cross sections below ~ 400 MeV. It is important to know to what extent this result indicates a "boundary" of validity of the DWIA for comparison with other types of observables. To date very little data is available near this energy. Recently, measurements of several inelastic transitions in ^{12}C have been made at Saclay[27] at $E_P = 402$ MeV. Figure 11 shows a comparison between DWIA results (425 MeV t matrix) using the CKWF and experimental data for the excitation of the 12.7 and 15.1 MeV states. These same two transitions at $E_P = 120$ MeV were described in Sec. III A 1.

Unlike the situation at 120 MeV, the cross section for the 12.7 MeV ($T = 0$) state is quite reasonably described by the DWIA at this higher energy without renormalization of the interaction (or transition density). Although the shapes of the calculated and experimental cross sections do not agree well in detail, they are in much better agreement than at lower bombarding energies. This transition is dominated by the noncentral parts of the force.

For the 15.1 MeV ($T = 1$) transition, the calculated cross section is in detailed agreement with the data for $q \lesssim 1$ fm^{-1}. At larger q the experimental cross section is underestimated. This deficiency in the CKWF at large q has been noted previously.[20] (Also see Sec. III A 1.)

These results suggest that the DWIA is of comparable validity at 120 and 400 MeV for $\Delta S = \Delta T = 1$ transitions at small q; for $\Delta S = 1$, $\Delta T = 0$ transitions, the DWIA appears considerably more reliable at the higher energy. Preliminary calculations for the 2^+ states at 4.44 ($T = 0$) and 16.1 ($T = 1$) MeV, however, suggest there may be problems. Data for these transitions are unavailable for publication at this time. Clearly more data near $E_P = 400$ MeV are needed before firm conclusions can be drawn.

C. Applications near 800 MeV

Data for the cases we will consider in this section have recently been taken at the Los Alamos Meson Physics Facility. The 800 MeV t matrix was used

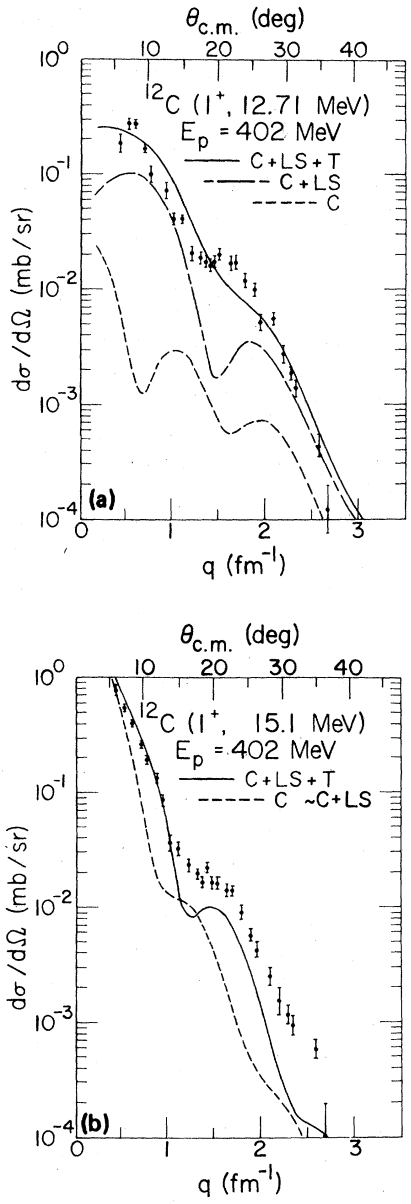

FIG. 11. Comparison of DWIA results (425 MeV t matrix) with experimental data for the excitation of the 12.7 and 15.1 MeV states in ^{12}C at $E_P = 402$ MeV. The CKWF were used.

and as mentioned earlier, it is likely to require significant updating when more complete $n + p$ amplitudes become available.

1. The $^{12}C(p,p')$ reaction at 800 MeV

Data for excitation of the 2^+ (4.44 MeV) (Refs. 28 and 29) and 1^+ (15.1 MeV) (Ref. 30) levels have recently been reported and are compared with DWIA calculations in Fig. 12. The CKWF were used for each of these transitions.

For the 2^+, $T = 0$ excitation, the DWIA cross section is seen to be in good agreement with the data out to $q \simeq 2$ fm^{-1} when the transition density is adjusted to reproduce the longitudinal form factor from (e,e') scattering. Although a slightly smaller value of b would improve the agreement, such an alteration would be inconsistent with e,e') data and might simulate some other deficiency. The calculated analyzing power is in good agreement with the data only for $q \lesssim 1$ fm^{-1}. Although there is qualitative agreement out to 3 fm^{-1}, the present results suggest an important deficiency in the present t matrix. A likely candidate is the N-N spin-orbit interaction whose isoscalar phase disagrees with those of present phenomenological optical potentials.

As at other bombarding energies, the shape of the 1^+ ($T = 1$) cross section is well reproduced for $q \lesssim 1$ fm^{-1}, where the calculated cross section is too small by $\sim 20\%$. The tensor force is important for $q \gtrsim 0.5$ fm^{-1}; the isovector spin-orbit part of the interaction is negligible.

Preliminary calculations for the 12.7 and 16.1 MeV levels are encouraging. These results will be reported elsewhere.

2. The $^{58}Ni(p,p')$ reaction at 800 MeV

It has been demonstrated[31] that the electromagnetic longitudinal ($C6$) and the transverse ($E6$) form factors for the transition to the 6^+ state at 5.125 MeV are well described by an isoscalar excitation involving only the $(f_{5/2}, f_{7/2}^{-1})$ configuration with a particle-hole amplitude of ~ 0.97. These form factors are well reproduced for $q \lesssim 2.5$ fm^{-1} using bare charges and g factors and an oscillator parameter of $b = 2.05$ fm. The simplicity of the tested wave functions for this transition, together with the availability of (p,p') data beyond $q = 3.5$ fm^{-1}, make this an appealing transition for studying the present N-N interaction at large momentum transfer. A study of this transition using an earlier version of the present t matrix has already been reported.[32]

Figure 13 shows a comparison of DWIA results with the experimental data using the pure isoscalar p-h transition density ($\times 0.97$). Overall the agreement is quite good; the data is not, however, reproduced in detail near $q = 1.4$ and 2.6 fm^{-1}. The discrepancy near 2.6 fm^{-1} is qualitatively similar to

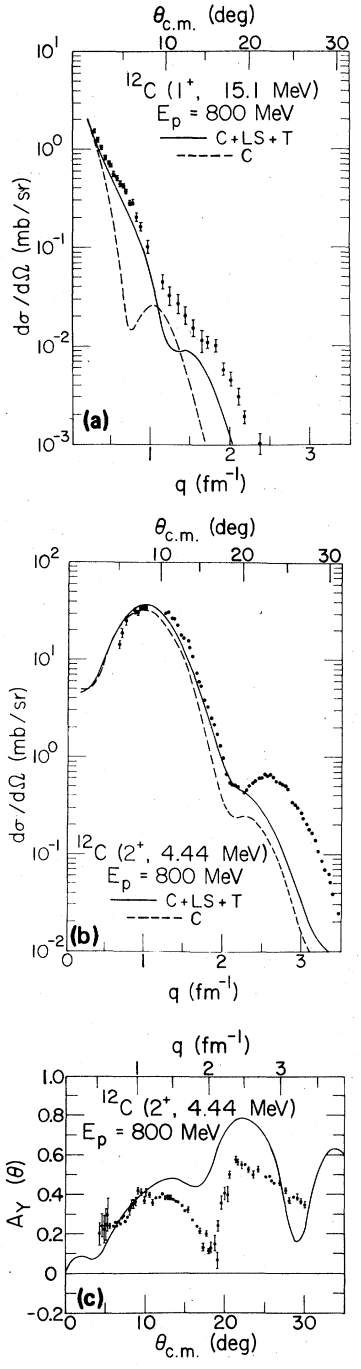

FIG. 12. Comparison of DWIA results (800 MeV t matrix) with experimental data for the excitation of the 4.44 (2^+) and 15.1 MeV (1^+) states in ^{12}C at $E_P = 800$ MeV. The calculated cross section for the 4.44 MeV state has been multiplied by 2 as is required to match the (e,e') longitudinal form factor. Multiplication of the DWIA cross section for the 15.1 MeV state by 1.2 would bring it into excellent agreement with the data for $q \lesssim 1$ fm^{-1}.

that noted above for the excitation of the isoscalar 2_1^+ state in ^{12}C at this same bombarding energy; the discrepancy near $q = 1.4$ fm^{-1} is harder to understand.

IV. SUMMARY

A local, energy-dependent representation of the free N-N interaction (t matrix) has been constructed from recently determined N-N amplitudes between 100 and 800 MeV for the purpose of calculating nucleon-nucleus scattering. Although the interaction becomes nonlocal when the knock-on exchange terms are included exactly, a short-range approximation may be used for the central and spin-orbit interaction for most transitions; this is especially true above ~ 150 MeV. This short-range approximation has been noted to be unreliable for calculating A_y near 120 MeV when convection currents contribute appreciably.

Both the techniques used to derive the present interaction and the multiple-Yukawa form assumed for it were chosen on the basis of anticipated applications, completeness of description, and convenience. A number of dynamical and symmetry properties of the interaction are discussed with respect to their possible implications for nucleon-nucleus scattering. Of particular interest is the dependence of the interaction upon bombarding energy which to some extent reveals the proton as a "tunable" probe of nuclear structure.

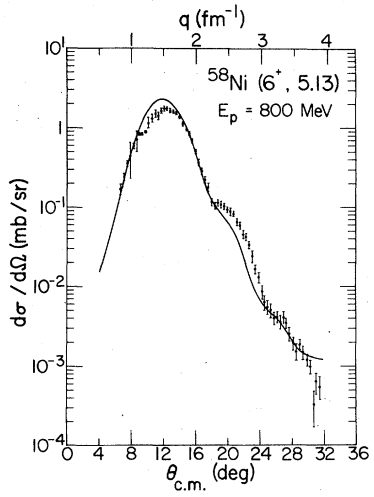

FIG. 13. Comparison of DWIA and experimental cross sections for the 6^+ level in ^{58}Ni at $E_x = 5.13$ MeV. The transition density was scaled to agree with the longitudinal form factor from (e,e').

Apart from the overall validity of the DWIA, it should be reemphasized that the present model of the t matrix is not entirely unique; some of the uncertainties in t are discussed and some of their consequences are noted. This problem clearly needs further study.

Although the emphasis here is not on analyzing specific experimental data, the interaction is illustrated through a number of applications to several types of transitions for which there exist both data and reasonable wave functions; these few illustrations in no way provide a thorough test of the force. There are some clear indications, however, of the need to refine the DWIA, particularly below 200 MeV where Pauli blocking is known to be important. At higher energies the present model (as expected) appears more quantitative. At essentially all energies considered, the DWIA appears to provide a good description of pionlike transitions ($\Delta S = \Delta T = 1$) at low momentum transfer.

In conclusion, the present interaction appears to provide a semiquantitative model for helping interpret nucleon-nucleus scattering microscopically and for qualitatively studying some of the most important probe characteristics of the (p,p') reaction at intermediate energies. Apart from refinements in the nuclear reaction theory, the present free interaction will have to be updated when more complete N-N data become available.

ACKNOWLEDGMENTS

We thank F. Petrovich and L. Ray for helpful discussions and suggestions. We also thank those experimentalists who provided us with early access to their data. We especially appreciate the help given to us by R. Arndt in using his phase shifts. This work was supported in part by the NSF and the DOE.

APPENDIX

Following Kerman, McManus, and Thaler (KMT) (Ref. 4) we show in this appendix how the central, spin-orbit, and tensor parts of the t matrix obtained in this work enter into the calculation of natural and unnatural parity excitations. This enables us to assess the relative importance of each part of t as a function of momentum transfer and bombarding energy as discussed in Sec. II B.

KMT show that, in the plane-wave impulse approximation, the differential nucleon-nucleus cross section for a specific angular momentum transfer (J) is given by

$$\frac{d\sigma}{d\Omega} = (|A|^2 + |C|^2) \times (\text{nuclear structure factor}) \tag{A1}$$

for natural parity excitations [$\Delta\pi = (-)^J$] in which only $\Delta S = 0$ to the target (no spin-transfer) is important and by

$$\frac{d\sigma}{d\Omega} = (|B|^2 + |C|^2 + |F|^2 + \xi|E|^2) \times (\text{nuclear structure factor}) \tag{A2}$$

for unnatural parity transitions [$\Delta\pi = (-)^{J+1}$] in which $\Delta S = 1$ is dominant. The amplitudes A, B, C, etc., are defined in Eq. (2) and ξ is a nuclear structure factor denoted by KMT as $2\rho/(1-\rho)$, which depends on the relative importance of the allowed orbital angular momentum transfers $L = J \pm 1$. When, as is often the case, $L = J - 1$ dominates (as is always the case for the excitation of stretched states), $\xi = 2J/(J+1)$.

The knock-on exchange terms are implicitly included in Eqs. (A1) and (A2). In the present approach we prefer (see Sec. II A) to include these terms explicitly, and this requires some modification or reinterpretation of these equations. The knock-on exchange contributions to the nucleon-nucleus amplitudes are evaluated in a short-range approximation[1,33] which is well established at intermediate energies for the central and spin-orbit parts of the interaction and appears to give a reasonable estimate of the exchange terms associated with the tensor force. This approximation (discussed briefly in Sec. II A) consists of replacing Q by k_A (the incident momentum in the nucleon-nucleus system) in Eq. (16) to obtain t^C, t^{LS}, and t^T appropriate for nucleon-nucleus collisions. In terms of these new t's Eqs. (A1) and (A2) become

$$\frac{d\sigma}{d\Omega} = (|t^C|^2 + |t^{LS}|^2) \times (\text{nuclear structure factor}) \tag{A3}$$

and

$$\frac{d\sigma}{d\Omega} = (|t^{LS}|^2 + |t^C + t^{T\alpha}|^2 + |t^C + t^{T\beta}|^2 + \xi|t^C + t^{T\gamma}|^2) \times (\text{nuclear structure factor}) , \tag{A4}$$

where

$$t^{T\alpha} = t^T(q) + (-)^l t^T(k_A) \ , \tag{A5a}$$

$$t^{T\beta} = -2t^T(q) + (-)^l t^T(k_A) \ , \tag{A5b}$$

$$t^{T\gamma} = t^T(q) - 2(-)^l t^T(k_A) \ , \tag{A5c}$$

corresponding to the tensor contribution to B, F, and E, respectively. Equations (A1)–(A4) are still schematic in the sense that t^C, t^{LS}, and t^T in Eq. (16) refer to states of definite spin and isospin in the N-N system. For use in nucleon-nucleus scattering where the transfer of definite quanta of spin and isospin is typical, it is useful to cast t in a form that displays this explicitly. If $\sigma(\tau)$ denotes the transfer of one unit of spin (isospin) we find:

$$\begin{aligned} t_0^C &= \tfrac{1}{16}(3t^{SE} + 3t^{TE} + t^{SO} + 9t^{TO}) \ , \\ t_\sigma^C &= \tfrac{1}{16}(-3t^{SE} + t^{TE} - t^{SO} + 3t^{TO}) \ , \\ t_\tau^C &= \tfrac{1}{16}(t^{SE} - 3t^{TE} - t^{SO} + 3t^{TO}) \ , \\ t_{\sigma\tau}^C &= \tfrac{1}{16}(-t^{SE} - t^{TE} + t^{SO} + t^{TO}) \ , \end{aligned} \tag{A6}$$

$$t_0^{LS} = \tfrac{1}{4}(t^{LSE} + 3t^{LSO}), \ t_\tau^{LS} = \tfrac{1}{4}(-t^{LSE} + t^{LSO}) \ ,$$

$$t_0^T = \tfrac{1}{4}(t^{TNE} + 3t^{TNO}), \ t_\tau^T = \tfrac{1}{4}(-t^{TNE} + t^{TNO}) \ ,$$

where, *SO*, *TE*, *LSO*, and *TNE* denote the singlet-odd, triplet-even (central), spin-orbit-odd, and tensor-even component of t and

$$t_\tau^{T\alpha} = \tfrac{1}{4}\{ -[t^{TNE}(q) + t^{TNE}(k_A)] + [t^{TNO}(q) - t^{TNO}(k_A)] \} \ , \tag{A7}$$

etc. From Eqs. (A3) and (A4) we see that the strength of the central (spin-orbit) part of the interaction for natural parity transitions is represented by $|t^C|$ ($|t^{LS}|$). For unnatural parity transitions the magnitudes of the central, spin-orbit, and tensor parts of the force as they enter into nucleon-nucleus collisions are given by $(2+\xi)^{1/2}|t_\sigma^C|$, $|t^{LS}|$, and $|\overline{t^T}| \equiv (|t^{T\alpha}|^2 + |t^{T\beta}|^2 + \xi|t^{T\gamma}|^2)^{1/2}$, respectively. For definiteness we have taken $\xi = 2$ in Fig. 1, which is most appropriate for the excitation of stretched high-spin states. As in Eq. (A7), the appropriate isospin combinations must be taken.

[1]F. Petrovich, H. McManus, V. A. Madsen, and J. Atkinson, Phys. Rev. Lett. 22, 895 (1969); W. G. Love, Nucl. Phys. A312, 160 (1978).

[2]W. G. Love and G. R. Satchler, Nucl. Phys. A159, 1 (1970); W. G. Love, *ibid.* A192, 49 (1972).

[3]G. Bertsch, J. Borysowicz, H. McManus, and W. G. Love, Nucl. Phys. A284, 399 (1977).

[4]A. K. Kerman, H. McManus, and R. M. Thaler, Ann. Phys. (N.Y.) 8, 551 (1959).

[5]A. B. Clegg and G. R. Satchler, Nucl. Phys. 27, 431 (1961); Mitsuji Kawai, Tukuo Terasawa, and Koichi Izumo, *ibid.* 59, 289 (1964).

[6]W. G. Love, in *The (p,n) Reaction and the Nucleon-Nucleon Force,* edited by C. D. Goodman *et al.* (Plenum, New York, 1980), p. 23; Proceedings of the LAMPF Workshop on Nuclear Structure with Intermediate-Energy Probes, Los Alamos, 1980 LASL, Report No. LA-8303C, p. 26; W. G. Love, Alan Scott, F. Todd Baker, W. P. Jones, and J. D. Wiggins, Jr., Phys. Lett. 73B, 277 (1978).

[7]F. Petrovich, in *The (p,n) Reaction and the Nucleon-Nucleon Force,* edited by C. D. Goodman *et al.* (Plenum, New York, 1980,) p. 115.

[8]F. Petrovich and W. G. Love, Nucl. Phys. A354, 499c (1981).

[9]J. Kelly *et al.,* Phys. Rev. Lett. 45, 2012 (1980).

[10]D. V. Bugg, J. A. Edgington, W. R. Gibson, N. Wright, N. M. Stewart, A. S. Clough, D. Axen, G. A. Ludgate, C. J. Oram, L. P. Robertson, J. R. Richardson, and C. Amsler, Phys. Rev. C 21, 1004 (1980).

[11]M. H. MacGregor, M. J. Moravcsik, and H. P. Stapp, Annu. Rev. Nucl. Sci. 10, 291 (1960).

[12]R. A. Arndt, private communication; M. H. MacGregor, R. A. Arndt, and R. M. Wright, Phys. Rev. 182, 1714 (1969).

[13]L. Ray, W. Rory Coker, and G. W. Hoffman, Phys. Rev. C 18, 2641 (1978); A. Chaumeaux, V. Layly, and R. Schaeffer, Ann. Phys. (N.Y.) 116, 247 (1978); W. G. Love, Phys. Lett. 26B, 271 (1968).

[14]R. Schaeffer and J. Raynal (unpublished); J. Raynal, Nucl. Phys. A97, 572 (1967).

[15]C. D. Goodman, C. A. Goulding, M. B. Greenfield, J. Rapaport, D. E. Bainum, C. C. Foster, W. G. Love, and F. Petrovich, Phys. Rev. Lett. 44, 1755 (1980).

[16]D. E. Bainum, J. Rapaport, C. D. Goodman, D. J. Horen, C. C. Foster, M. B. Greenfield, and C. A. Goulding, Phys. Rev. Lett. 44, 1751 (1980); D. J. Horen, C. D. Goodman, C. C. Foster, C. A. Goulding, M. B. Greenfield, J. Rapaport, D. E. Bainum, E. Sugarbaker, T. G. Masterson, F. Petrovich, and W. G. Love, Phys. Lett. 95B, 27 (1980); B. D. Anderson, J. N. Knudson, P. C. Tandy, J. W. Watson, R. Madey, and C. C. Foster, Phys. Rev. Lett. 45, 699 (1980).

[17]S. Yen, R. J. Sobie, T. E. Drake, A. D. Bacher, G. T. Emery, W. P. Jones, D. W. Miller, C. Olmer, P. Schwandt, W. G. Love, and F. Petrovich, Phys. Lett.

(to be published); Alan Scott, F. Todd Baker, M. A. Grimm, Jr., J. H. Johnson, V. Penumetcha, R. C. Styles, W. G. Love, W. P. Jones, and J. D. Wiggins, Jr., *ibid.* 45, 1315 (1980); J. Comfort, private communication.

[18]J. M. Moss, C. Glashausser, F. T. Baker, R. Boudrie, W. D. Cornelius, N. Hintz, G. Hoffman, G. Kyle, W. G. Love, A. Scott, and H. A. Thiessen, Phys. Rev. Lett. 44, 1189 (1980).

[19]E. J. Squires, Nucl. Phys. 6, 504 (1958).

[20]J. R. Comfort, S. M. Austin, P. T. Debevec, G. L. Moake, R. W. Finlay, and W. G. Love, Phys. Rev. C 21, 2147 (1980); J. R. Comfort, R. E. Segel, G. L. Moake, D. W. Miller, and W. G. Love, *ibid.* 23, 1858 (1981).

[21]S. Cohen and D. Kurath, Nucl. Phys. 73, 1 (1965); J. B. McGrory, private communication.

[22]J. B. Flanz, Ph.D. thesis, University of Massachusetts (University Microfilms, Ann Arbor, 1979); J. B. Flanz, R. S. Hicks, R. A. Lindgren, G. A. Peterson, A. Hotta, B. Parker, and R. C. York, Phys. Rev. Lett. 41, 1642 (1978).

[23]S. Yen *et al.*, Phys. Lett. 93B, 250 (1980).

[24]N. Hintz, private communication.

[25]W. G. Love (unpublished).

[26]L. Ray, Phys. Rev. C 20, 1857 (1979).

[27]J. L. Escudié *et al.*, Phys. Rev. C (to be published).

[28]G. S. Blanpied *et al.*, Phys. Rev. C 18, 1436 (1978).

[29]R. P. Liljestrand *et al.*, Phys. Rev. Lett. 42, 363 (1979).

[30]M. Haji-Saeid, C. Glashausser, G. Igo, W. Cornelius, M. Gazzaly, F. Irom, J. McClelland, J. M. Moss, G. Pauletta, H. A. Thiessen, and C. A. Whitten, Jr., Phys. Rev. Lett. 45, 880 (1980).

[31]R. A. Lindgren, J. B. Flanz, W. J. Gerace, R. S. Hicks, A. Hotta, D. Huse, G. A. Peterson, and R. C. York, Phys. Rev. Lett. 41, 1705 (1978).

[32]G. S. Kyle *et al.*, Phys. Lett. 91B, 353 (1980).

[33]J. Raynal, in *Proceedings of Conference on Certain Microscopic Aspects of Nuclear Reactions, La Toursinei, France* (Institute of Nuclear Physics, Vieleurbanne, France, 1971).